Proceedings of ASME 2012 31st International Conference on Ocean, Offshore and Arctic Engineering
OMAE 2012
July 1-6, 2012, Rio de Janeiro, Brazil

OMAE2012-84101

LIFECYCLE FATIGUE LOAD SPECTRUM ESTIMATION FOR MOORING LINES OF A FLOATING MARINE ENERGY CONVERTER

Philipp R. Thies *
University of Exeter
College of Engineering, Mathematics and Physical Sciences
Penryn, Cornwall, TR10 9EZ, UK

Lars Johanning
George H. Smith
University of Exeter
College of Engineering, Mathematics and Physical Sciences
Penryn, Cornwall, TR10 9EZ, UK

ABSTRACT

One of the key engineering challenges for the installation of floating marine energy converters is the fatigue of the load-bearing components. In particular the moorings which warrant the station-keeping of such devices are subject to highly cyclic, non-linear load conditions, mainly induced by the incident waves.

To ensure the integrity of the mooring system the lifecycle fatigue spectrum must be predicted in order to compare the expected fatigue damage against the design limits. The fatigue design of components is commonly assessed through numerical modelling of representative load cases. However, for new applications such as floating marine energy converters numerical models are often scantily validated.

This paper describes an experimental approach, where load measurements from tank tests are used to estimate the lifecycle fatigue load spectrum for a potential deployment site. The described procedure employs the commonly used Rainflow cycle analysis in conjunction with the Palmgren-Miner rule to estimate the accumulated damage for individual sea states, typical operational years and different design lives.

This allows the fatigue assessment of mooring lines at a relatively early design stage, where both information from initial tank tests and the wave climate of potential field sites are available and can be used to optimise the mooring design regarding its lifecycle fatigue conditions.

keywords: reliability, fatigue, rainflow, mooring, fatigue

NOMENCLATURE

s scaling factor
WEC Wave Energy Converter
OWC Oscillating Water Column
A Anchor point
WP Wave probe
S stress amplitude
S_∞ fatigue limit
RFM Rainflow Matrix
H_s significant wave height
T_p wave peak period
F_{Moor} measured mooring force [N]
A cross-sectional area [mm^2]
σ_{NOM} nominal stress [MPa]
M multiplication factor for rainflow matrix

1 INTRODUCTION

Marine renewable energy is envisaged to play an important role as a future energy source. For the UK it is estimated that wave and tidal energy could provide up to 17% of the current electricity demand [1]. This would help to guarantee the security of energy supply and significantly reduce carbon emissions. Beyond that, marine renewable energy holds the opportunity to create a new and successful UK industry sector estimated to be worth 15 billion [2]. From an engineering point of view though, marine energy is one of the least developed renewable energy technologies and has to be regarded as unproven. The main en-

*Address all correspondence to this author. Email: P.R.Thies@exeter.ac.uk

gineering challenge is being identified as the reliability of components and devices [3–5].

In order to utilise the large majority of this estimated resource, floating offshore installations will be required. This makes the mooring system an indispensable component for a successful and safe operation for floating marine energy converters.

From a reliability perspective, two criteria have to be met during the mooring load analysis. Firstly, the peak loads must not exceed the the maximum strength of the moorings and secondly, the cyclic loading needs to be assessed to ensure that the fatigue design is satisfactory. Mooring fatigue is a failure mode of particular concern for floating marine energy applications [6–8] as the operating wave environment induces highly cyclical load conditions.

This paper presents an effort to quantify the life cycle fatigue load spectrum that may be expected for mooring lines of a floating marine energy converter. Rather than numerical simulations, experimental measurements from a 1:20 scale tank test are being used to derive a load spectrum estimate.

While the procedure is applicable to other types of marine energy devices, exemplary results are presented for a generic floating wave energy converter. The load spectrum is determined for an assumed full-scale installation at the Wave Hub site in the South West of the UK, where commercial-scale installations are being planned during 2012 [9].

The paper broadly falls into three main parts. In section 2 the experimental setup is briefly presented, including the energy converter and the range of tested sea states. Section 3 then describes the approach that is applied to estimate the annual field load conditions from the experimental tests. In section 4 the main results that emerge from the analysis are shown.

2 EXPERIMENTAL SETUP

As part of the SuperGen Marine initiative, physical model tests of a generic floating wave energy converter (WEC) were carried out in the NTNU Trondheim wave basin, funded by the European programme Hydralabs III. The test objectives were to gather data which would serve the validation of numerical models and to investigate potential interactions when the devices are deployed in array configuration [10–12].

2.1 Wave Tank

Figure 1 illustrates the experimental setup in the tank, the definition of the coordinate system and the mooring configuration. The device (WEC1) is moored to the bottom of the tank with three mooring lines attached to welded anchor positions (A1, A2, A3). The water depth is set to 2.8m and the surge motion of the WEC device (x-axis) has been defined positive in opposition to the wave maker.

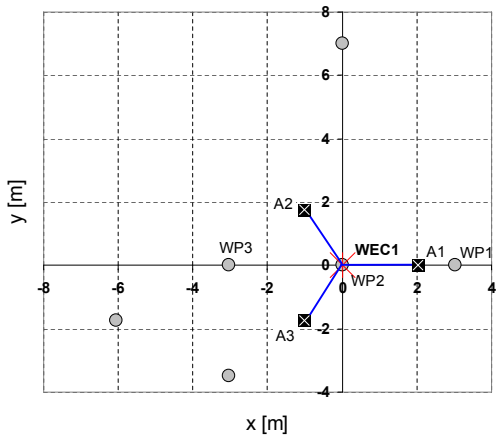

FIGURE 1. COORDINATE SYSTEM SHOWING WAVE PROBES (WP), ANCHOR POINTS (A) and CONVERTER LOCATION (WEC)

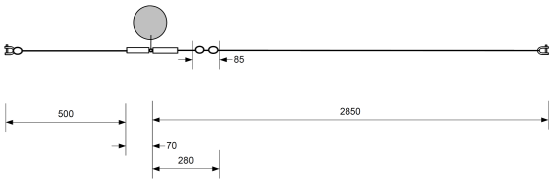

FIGURE 3. MOORING LINE ARRANGEMENT, DIMENSIONS IN [mm]

2.2 Generic Wave Energy Converter

The wave energy converter used in the tests is a cylindrical floating device of the Oscillating Water Column (OWC) type (see Fig. 2). The power take-off was modelled with an orifice plate at the top of the cylinder. The WEC was moored with three mooring lines, which incorporate a top floater each and where attached via shackles to the WEC and the anchoring point. The mooring line consisted of 3 Strand Aramid Core rope with a 16 plait polyester cover of a diameter $d_{line,model} = 3.5mm$. To estimate the forces under full-scale conditions, Froude's scaling law is used, which applies to most wave energy applications as the relative influence of viscous forces F_v is small in comparison to the influence of the gravitational force F_g. This is the case when the modelled device has a compact form, i.e. a the wetted surface area is small in relation to the immersed volume [13]. The physical dimensions of the 1/20 model and the associated full-scale values are shown in Tab. 1. The mooring line arrangement is depicted in Fig. 3.

2.3 Instrumentation and Test Regime

The experiment was extensively instrumented to determine the wave conditions, the converter movements in all six degrees of freedom, the mooring forces and power absorption. For the one device considered here this comprises (compare Fig.2):

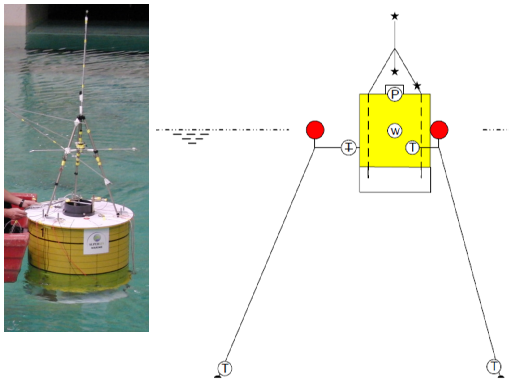

FIGURE 2. SIDE VIEW AND INSTRUMENTAION OF GENERIC WAVE CONVERTER

TABLE 1. DIMENSIONS AND FROUDE SCALING, $s = 20$

Dimension	Unit	Model	Scaling	Full scale
Height	[m]	1.1	s	22
Diameter	[m]	0.8	s	16
Water depth	[m]	2.8	s	56
Displacement force	[kN]	0.85	s^3	6800
Mooring line diameter	[mm]	3.5	s	70
Mooring elastic modulus E	[GPa]	13.8	s	276
Natural period in heave $T_{n,heave}$	[s]	4.02	$\sqrt{s}$	18

- 6 wave probes
- 1 internal water level sensor
- 1 pressure transducer
- 6 mooring line load cells
- 1 non contact motion tracking system

Two test regimes are considered in this paper, namely i) tests in regular (monochromatic) waves and ii) tests in irregular (polychromatic) waves. The simulated sea states at full scale conditions have a significant wave height of $H_s = 2-6m$ and a wave peak period $T_p = 5-13s$. The actual simulated sea states are depicted in Fig. 4. The test duration for regular waves was set to $t_{reg} = 6min$ while irregular sea states were simulated for $t_{irreg} = 27min$. In between sea states the tank was left to settle for $t_{settle} = 15min$. It is worth noting, that the OWC is considered to be operational in the largest sea states tested. Thus, hydrodynamic characteristics in a possible 'survival mode' of the device are not considered in the following.

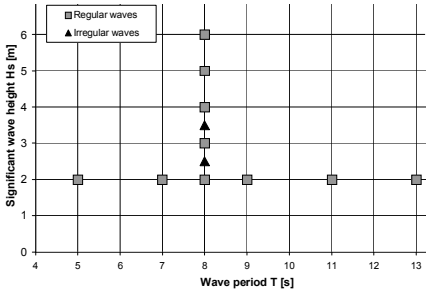

FIGURE 4. SIMULATED SEA STATES

Figure 5 plots a 500s window with a high tension, snap load event at around 3,630s. It is evident that the device motion is a superposition of low- and high-frequency components. The translational motions are dominated by heave and surge components while there is only a limited amount of sway. It is also shown that there is a significant offset in the X position which is due to the incoming waves which push the device back from its origin position. For the rotational motions pitching and rolling motions are more pronounced with amplitudes of up to 20°. Under the simulated conditions sway motion is small. While this type of plot gives some information about the prevalent device motions it is difficult to identify the motion characteristics that are associated with high load events for the entire time series.

3 FATIGUE LOAD ANALYSIS

There are different methods to characterise the fatigue potential of load signals [14]. Common methods are level crossing and range counting procedures where the load signal is assessed regarding the crossing of a specific reference level or its load

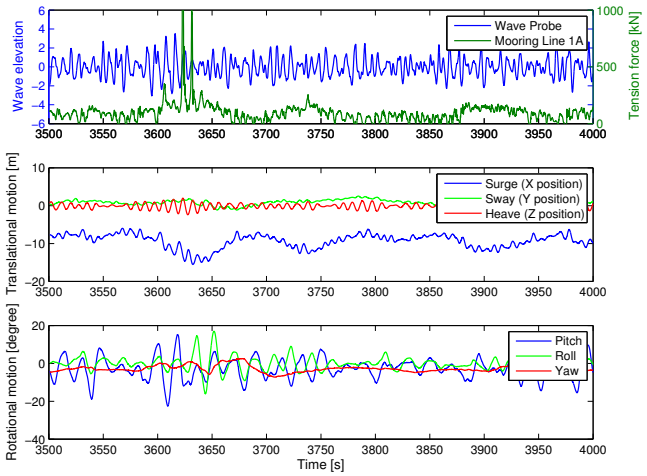

FIGURE 5. Wave elevation, mooring tension force and device motion, $H_s = 3.5m$, $T_p = 8s$

amplitudes. When the load cycles are of randomly varying amplitude the so-called rainflow count method is commonly used to evaluate fatigue damage, as it realistically considers the fatigue damage caused by each, individual load cycle. It identifies and counts the stress ranges corresponding to individual hysteresis loops. Thus, the rainflow cycle count methodology is used here.

3.1 Rainflow Cycle Method

The rainflow algorithm is based on the definition for a rainflow cycle [15], see Fig.6. Starting from a local load maximum Max_K the region to the left and the right, which are characterised by lower load levels than Max_K are determined. Two minima are identified before and after Max_K, i.e. Min_{K+} and Min_{K-}. That minimum having the smaller deviation from Max_K is chosen as the rainflow minimum $Min_{K,RFC}$, giving the k:th rainflow cycle $(Min_{K,RFC}, Max_K)$. This algorithm is then repeated over the entire time series t.

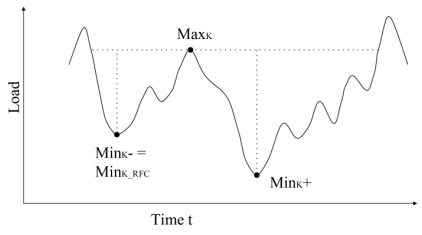

FIGURE 6. RAINFLOW CYCLE COUNT DEFINITION [15]

Further, with t_K as the time of the k:th local maximum and the rainflow amplitude characterising the amplitude of the hysteresis loop the total damage $D(t)$ can be calculated by the Palmgren-Miner rule. It is also known as the linear cumulative fatigue damage rule and assumes that the each load cycle causes a damage of $1/N(S_{K,RFC})$. Using this linear cumulative rule, a failure occurs if $D \geq 1$. The fatigue damage $D(t)$ is calculated as the sum of the individual blocks of constant load amplitude blocks:

$$D(t) = \sum_{t_k \leq t} \frac{1}{N(S_{K,RFC})} = \frac{1}{K} \sum_{t_k \leq t} (S_{k,RFC})^{\beta} \tag{1}$$

Where $N(S_{K,RFC})$ is the number of cycles during the time t. K represents a random variable to account for material uncertainties and β is usually taken to be a fixed constant, describing the shape of the material's S-N curve:

$$N(S) = \begin{cases} K \cdot S^{-\beta} & S > S_{\infty} \\ \infty & S \leq S_{\infty} \end{cases} \tag{2}$$

With $N(S)$ number of load cycles; S stress amplitudes; S_{∞} fatigue limit

For the mooring materials considered later, β is in the range from 3 to 5. Therefore, following Equ.1, a doubling of the load amplitude leads to an increase of fatigue damage by a factor of between 8 and 32. Hence, the fatigue damage is mainly caused by the largest load cycles.

3.2 Mooring Line Fatigue Characteristics

The two primary factors to affect fatigue reliability are the material's fatigue strength and the applied cyclic loading. While the fatigue strength is an intrinsic material and mechanical characteristic, the applied loading describes an extrinsic process. Two approaches are common to evaluate a material's fatigue reliability [16]: The crack growth model examines the fracture behaviour of mechanical elements under dynamic loading, where failures occur if dominant cracks have grown to a critical length. The stress-life (S-N) approach considers the cumulative fatigue damage, where a failure occurs after a number of loading cycles N, at a particular stress range S.

S-N curves describe the fatigue properties of different materials. These curves are found empirically through fatigue tests and show the number of cycles to failure N, as a function of the cyclic stress S. The fatigue life design for offshore structures is commonly based on the use of S-N diagrams [17], which will thus be used in the following. Fatigue curves are modelled with a power law, that stems from the linear regression of fatigue test results. The number of cycles $N(S)$ to failure for a particular cyclic stress range S is described by Equ.3.

$$N(S) = KS^{-\beta} \tag{3}$$

$$log\,(N(S)) = log\,(K) - \beta \cdot log\,(S) \tag{4}$$

Where $N(S)$ is the number of cycles at a certain stress, S is the constant amplitude cyclic stress, K is the intercept parameter of the S-N curve and β describes the slope of the S-N curve.

The parameters for design S-N curves for tension-tension fatigue of different mooring line materials are given in the DNV standard for position mooring [18] and are plotted in Fig.7. The graph shows the reference fatigue design curves for steel wire ropes and chain. The given curves imply that the chain is exposed to the corrosive influence of seawater, while the curves for steel wire rope assume corrosive protection, e.g. through outer sheath lining. From the four mooring types spiral steel wire rope has the most favourable fatigue properties followed by the stranded wire, the studded- and the studless chain.

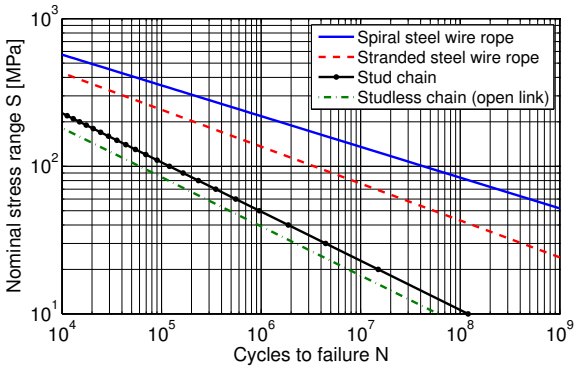

FIGURE 7. NOMINAL S-N FATIGUE CURVES FOR DIFFERENT MOORING MATERIALS

As the S-N curves are given in terms of the nominal stress range, the measured tension load signal is converted to a nominal stress using:

$$\sigma_{NOM} = \frac{F_{Moor}}{A} \tag{5}$$

σ_{NOM} is the nominal stress [MPa], F_{Moor} is the measured mooring force [N] and A is the cross-sectional area of the mooring line [mm^2].

3.3 Cycle Count and Damage Estimation

The rainflow cycle analysis of the mooring tensions has been carried out with the WAFO Matlab toolbox [19]. The calculation comprises two subsequent steps for the each measured load time history of the individual sea states. Only the leading mooring line (L1A) is considered as it carries the main load.

1. Rainflow cycle count to compute rainflow matrix, showing the amount of load cycles for different stress ranges.
2. Fatigue damage calculation, which computes the accumulated damage, based on the rainflow matrix and the fatigue properties of the mooring line..

The rainflow matrix counts each range in the interval the cycle started (Min) and the value where the cycle is completed (Max). The number of occurrence indicates the number of observed load cycles in the specific range. Additionally a rainflow filter is used to reduce signal noise exclude load cycles with a tension force $F \leq 50kN$ as these load cycles are too small to induce any fatigue damage. The generated rainflow matrix forms the basis of the fatigue damage calculation, as defined by the Palmgren-Miner rule in Equation 1.

Both the filtered rainflow matrix and the corresponding fatigue damage matrix for a simple chain during one particular sea state are shown in Figure 8. Both matrices have the same structure, as the fatigue damage calculation is based on the rainflow matrix. The cycles in the upper left corner are those with the largest amplitudes ($> 250MPa$ nominal stress in the chain) and thus result in the largest fatigue damage for this sea state. This analysis is repeated for each of the sea states that have been tested.

3.4 Estimation Of Annual Load Conditions

After the load conditions have been assessed for individual sea states, the question arises how this corresponds to actual field load conditions. More precisely, how can the fatigue life be estimated using the available data? This section aims to estimate the annual field load conditions with regard to mooring line tensions, if the full-scale version of the OWC device would be deployed at a particular site.

3.4.1 Annual load spectrum generation Some additional information and subsequent calculations are needed to generate an annual load spectrum from the individual sea states. Firstly, the annual wave characteristics of the deployment site are required. As a second step, the probability of each sea state is assigned to the experimental sea states. The objective is to derive a multiplicative factor for each experimental sea state, in order to estimate the annual wave climate at the site regarding the accumulated load cycles, using the available experimental load data, such that:

$$P_{site}(H_s, T_p) \mapsto RFM_{test}(H_s, T_p) \cdot M \tag{6}$$

where $P_{site}(H_s, T_p)$ is the annual probability of a given sea state at the site (specified through H_s and T_p), $RFM_{test}(H_s, T_p)$ is the

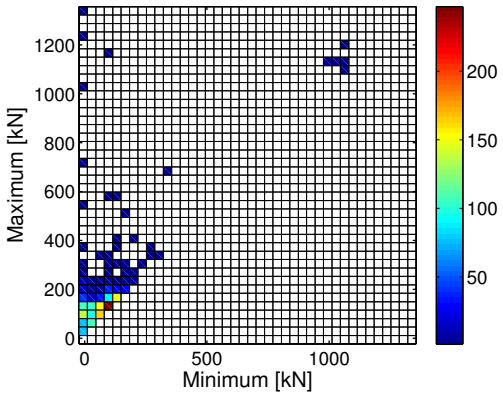

(a) Filtered rainflow matrix

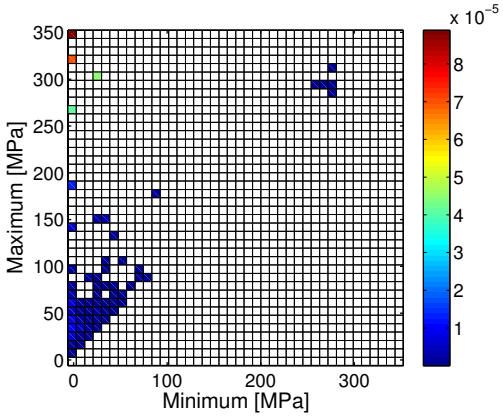

(b) Damage matrix

FIGURE 8. RAINFLOW CYCLE AND DAMAGE MATRIX
$H_S = 3.5m$, $T_p = 8.0s$. Damage results shown for studless chain with $K = 6 \cdot 10^{10}$ and $\beta = 3$.

calculated rainflow matrix of the experimental test and M is the adjusting multiplying factor with

$$M = P_{assign}(H_s, T_p) \cdot 8760h\frac{1}{2} \tag{7}$$

$P_{assign}(H_s, T_p)$ is the assigned annual probability for an experimental sea state, effectively this is the sum of $P_{site}(H_s, T_p)$ assigned to an experimental sea state. The factors relate to the number of hours for a year (8760h) and account for the fact that the RFMs are calculated for 2 hour intervals.

One difficulty that is likely to arise here is that the experimental tests do not cover the entire range of sea states. The wave climates used below contain 40 different sea states. These are already classified trough bins (typically H_s interval of $0.5m$ and T_p interval of $1s$) and thus are a simplification of the actual occurring wave conditions. However, experimental load cases may be even less than the number of populated scatter bins. This is the case for the experimental data, which investigated a total of 12 different sea states. In order to still estimate the expected annual load spectrum two approaches have been followed:

1. Calculation of a fractional year, that is representative of the experimentally tested conditions
2. Estimation of full annual spectrum through reducing the wave conditions to wave height H_s only, i.e. assigning P_{site} irrespective of T_p.

The first approach adheres to the available data and should thus yield a sound estimate of expected loads for the fraction of the year where sea states are similar to the experimental conditions. However, if experimental data is scarce no annual load estimate can be derived. If the assumption is acceptable, that the majority of fatigue damage is associated with increased wave heights rather than the incident wave period, the annual load spectrum may be estimated with the second approach. For the data at hand this showed to be a reasonable assumption.

During the experimental tests the wave period was only varied for $H_s = 2m$ but not for larger wave heights, leading to the situation where not all scatter cells are populated. However, comparing the influence of H_s and T_p on the accumulated fatigue damage for the experimental tests, the variation of wave heights showed to have the dominant influence compared to variations in wave period (comp. Fig.10).

3.4.2 Case study - Wave climate parameters To provide an example here, the operational fatigue loads have been calculated for a representative field site, where annual wave characteristics are readily available and device installations are envisaged. The site for the case study was chosen as the WaveHub site off the Northern coast of Cornwall, UK [9]. A scatter plot that is derived from a measurement campaign during 2005-2006 is published in [20]. For the same site a long term wave climate has been predicted by [21] who used the measured data in conjunction with modelled wave data (from a 18 year period) in a Measure-Correlate-Predict analysis. The long term estimate will be used in the following as it describes the long-term average wave conditions and is thus better suited to assess the long-term fatigue conditions. As the experimental tests are not available for the desired range of sea states, covering all combinations of period *and* wave height, the wave climate is curtailed to the probability distribution of the significant wave height, H_s. The wave climate with regard to H_s that is used for the following calculations is shown in Fig. 9.

Each experimental test is assigned an annual probability, P_{assign}, that corresponds to the same wave height in the scatter plot. The assignment for each experimental sea state is tabulated in Tab.2. P_{assign} represents the assigned annual probability of

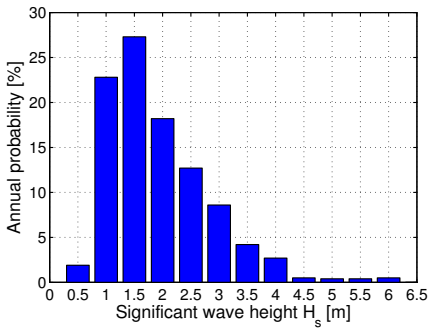

H_s [m]	P_{annual} [%]
6.0	0.5
5.5	0.4
5.0	0.4
4.5	0.5
4.0	2.7
3.5	4.2
3.0	8.6
2.5	12.7
2.0	18.2
1.5	27.3
1.0	22.8
0.5	1.9
Total	100.0

FIGURE 9. ANNUAL PROBABILITY DISTRIBUTION OF WAVE HEIGHTS NEAR WAVE HUB SITE [21]

TABLE 2. ASSIGNMENT OF ANNUAL PROBABILITIES

i	Test	$H_s[m]$	P_{assign} [%]	M
1	2020	2	82.8	3626
2	2060	3	12.7	559
3	2070	4	3.2	141
4	2080	5	0.8	33
5	2090	6	0.5	21

the experimental test condition and M denotes the multiplication factor for the corresponding rainflow matrix.

The annual load cycle matrix is then computed as:

$$\sum_{i=1}^{i=5} RFM(H_s) \cdot M_i \tag{8}$$

Where i denotes the corresponding sea state. The estimated annual field load conditions can thus be thought of as a linear combination of individual experimental sea states.

4 RESULTS

In this section the numerical results of the above case study are presented. It must be noted that these findings are specific to the generic device and the taut mooring configuration. The results cannot be directly transferred to other types of devices. However, the approach and analysis may well be applied to other marine energy converters in order to estimate the expected fatigue damage for a particular configuration and potential deployment site. Three aspects are presented, the fatigue damage caused by individual seastates, the estimated annual mooring load spectrum and the resulting annual accumulated fatigue damage for different mooring materials.

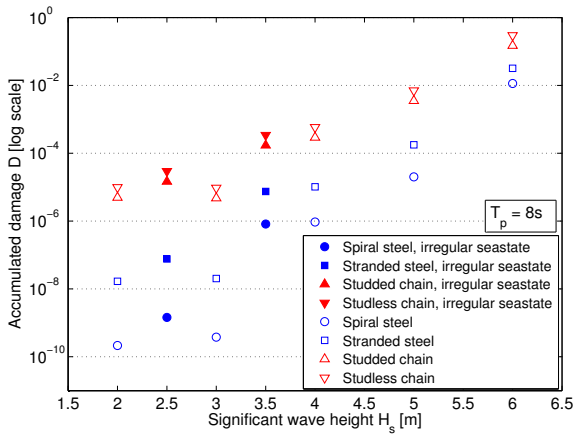

FIGURE 10. MOORING LINE FATIGUE DAMAGE FOR DIFFERENT WAVE HEIGHTS H_s.
Duration of sea state $t = 2h$, wave period $T_p = 8s$.

4.1 Damage For Individual Seastates

The rainflow analysis procedure described above has been applied to the range of experimentally tested seastates. The accumulated damage for each sea state is calculated. Two different mooring lines are considered under full-scale conditions, steel wire rope (in spiral and stranded configuration) and steel chain (in studless and studded configuration). The S-N material properties are derived from Fig.7. The accumulated fatigue is calculated for a two hour interval of each sea state. This then allows a comparison of the resulting fatigue damage with regards to incident wave height H_s and wave period T_p.

Figure 10 shows the accumulated fatigue damage D plotted against the significant wave height H_s for steel wire and chain configurations. A logarithmic scale has been applied for D to allow the large range of values to be displayed. The solid markers show values for irregular sea states. It is apparent, that the fatigue damage drastically increases with higher H_s. This is attributed to the occurrence of snap loads which were identified in particular for wave $H_s > 3m$ and account for the majority of the caused fatigue damage. Thus, for $H_s = 6m$ the studless chain consumes almost 30% of its fatigue life, while for $H_s = 2m$ it consumes only 0.01%. The spiral steel wire exhibits a better fatigue life performance and consumes 1% and $2 \cdot 10^{-8}$ % of its fatigue life at $H_s = 6m$ and $H_s = 2m$ respectively.

Another observation is that the spread of damage values for the different mooring materials and configurations declines for larger wave heights. Still the ranking order that steel wire shows the better fatigue behaviour over chain is consistent.

4.2 Annual Load Spectrum

The annual tension load spectrum for the leading mooring line is calculated as linear combination of the individual experi-

mental sea states. It comprises all load cycles the mooring line would experience for a typical year of operation at the chosen deployment site.

The presented analysis only considers the fatigue damage estimated from the tension measurements in regular waves. It must be noted that the wave heights for regular and irregular sea states are not equivalent. The wave height for regular sea states is twice the amplitude of the sinusoidal, while the significant wave height H_s in irregular seas denotes the mean of the highest one thirds of encountered wave heights.

An equivalent wave height H_{eq} which represents the sinusoidal equivalent signal of an irregular sea state, has been defined [22] as $H_{eq} = \frac{H_s}{\sqrt{2}}$.

The assumption made for the annual load spectrum is that a fatigue estimate based on regular sea states applies to a scatter plot of real, irregular sea states. In principle this leads to an overestimate of the applicable equivalent wave height by a factor of $\sqrt{2}$. Yet, as can be seen from Fig. 10 the fatigue damage for the irregular seas is larger than the the damage encountered for regular sea states. This is due to the fact that the fatigue damage is mainly governed by the largest wave height and the non-linear snap load events during each sea state, not the mean or equivalent wave height. It must thus be noted, that the annual load spectrum is a coarse estimate, based on regular sea state measurements. The presented estimates are therefore deemed to be optimistic compared to the results expected for a set of irregular sea states. However, this uncertainty may be considered to be accounted for in the safety factors referred to in Sec. 3.4.

Figure 11 shows the annual load spectrum in form of the rainflow matrix (11(a)) and the distribution of load amplitudes (11(b)). In the rainflow matrix, those load cycles with a large tension range, i.e. small minima and high maxima, are plotted to the left of the matrix. Cycles with smaller load ranges at a higher load level, are plotted near to the centre of the matrix. The amplitude distribution plot shows the occurrence of different load amplitudes. It gives a better view of the number of cycles at different load magnitudes. The total number of cycles amounts to $N_{annual} = 3.29 \cdot 10^6 \backslash year$. The smallest load amplitudes ($< 50kN$) are estimated to occur about in the order of 10^6 times a year while the largest amplitudes ($> 900kN$) are expected to occur in the order of 10^3. The largest amplitudes do not follow the overall trend, as they are caused by snap loads which occur in all sea states.

4.3 Annual Accumulated Fatigue Damage

The annual damage matrix has the same pattern as the the underlying rainflow matrix. It differs with regard to the stress ranges which are converted to the nominal stress (MPa) of the mooring line and the colour bar, which represents the accumulated fatigue damage for each cell.

Figure 12 depicts the damage matrix for spiral steel wire which exhibits the best fatigue properties of the mooring materials compared here. The total accumulated annual fatigue damage is estimated as $D_{annual} = 6.96 \cdot 10^{-3}$. The majority of the fatigue damage stems from the largest amplitude cycles ($\sigma_{NOM} > 250MPa$) which contribute a total damage of $D = 5.34 \cdot 10^{-3}$, accounting for over 75% of the annual fatigue damage.

TABLE 3. ESTIMATED ACCUMULATED FATIGU DAMAGE D FOR DIFFERENT MOORING LINES AND DESIGN YEARS; $D \geq 1$ INDICATES FATIGUE FAILURE

Design years	Spiral steel	Stranded steel	Studded chain	Studless chain
1	0.01	0.05	0.65	1.30
5	0.03	0.23	3.26	6.52
10	0.07	0.46	6.52	13.05
15	0.10	0.69	9.79	19.57
20	0.14	0.92	13.05	26.10

The estimated fatigue damage for the different mooring lines is tabulated in Tab.3. It is a projection of the estimated annual fatigue damage for a number of years, assuming that the typical year reoccurs. In reality there would be inter annual variations, but as the long term wave climate was used here, it is reasonable to calculate on the basis of the average year to obtain an indication of damage fatigue for different design year projections.

Spiral steel wire performs well and remains within the design limit for fatigue. Stranded steel wire comes close to $D = 1$ in the 20 year case. The chosen chain diameter seems to be inappropriate for the modelled application. This is mainly due to the high snap loads. Again it should be noted here, that these figures should be treated with caution, as they are very specific to the modelled device and are subject to the assumptions made in the calculations.

The safety factors for the fatigue limit state (FLS) are specified in [18] and typically range between 1 and 10 for steel moorings. Considering the highest safety actor, only the spiral steel mooring would be within the fatigue limit for the 5 and 10 year case.

It is of interest to assess the composition of the total fatigue damage, i.e. which sea states have caused the most severe fatigue damage. Those load conditions could then e.g. be replicated in service simulation tests as described in [23,24]. The contribution to the total fatigue damage for each type of mooring line is shown in Fig.13. The bars are grouped for each sea state, while the different patterns indicate the mooring material. The contributions for each mooring type sum up to 1, which is the reference value given in Tab.3. The largest sea state with $H_s = 6m$ clearly causes the most severe fatigue damage (between 72% and 88% of the

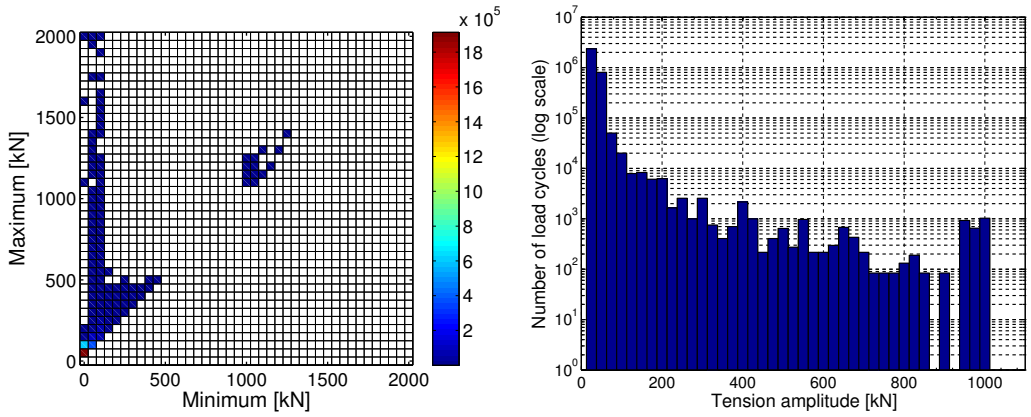

(a) Rainflow matrix (b) Amplitude distribution

FIGURE 11. ANNUAL LOAD SPECTRUM LEADING MOORING LINE; IRRESPECTIVE OF T_p

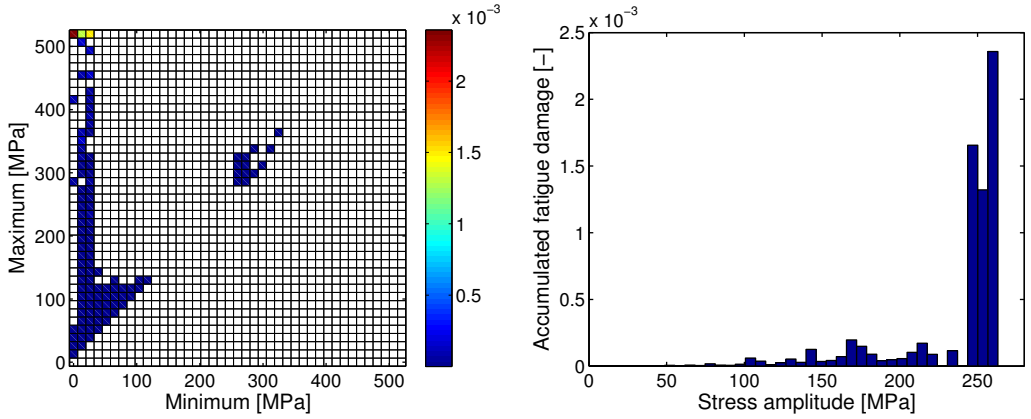

(a) Damage matrix (b) Stress amplitudes

FIGURE 12. ANNUAL DAMAGE MATRIX FOR SPRIAL STEEL MOORING LINE; TOTAL ACCUMULATED DAMAGE $D_{annual} = 6.96 \cdot 10^{-3}$

total annual damage), irrespective of the mooring type. The contribution for $H_s = 5m$ ranges between 10% and 19% of the total damage. Thus, these two sea states alone cause over 90% of the fatigue damage.

5 CONCLUSION

The paper has presented a practical approach to estimate the lifecycle fatigue damage for the mooring components of a floating WEC from experimental data. The findings highlight that fatigue considerations are crucial for marine renewable applications which operate in the wave environment, as cyclic loadings are very high and fatigue limits may be quickly exceeded under operational wave and load conditions. The information that is obtained through this analysis would help to reiterate or approve the fatigue design of components at a relatively early stage in the design process. Hence cost-implications of a change in design are limited.

ACKNOWLEDGMENT

The first author would like to acknowledge the funding provided by the UK Centre for Marine Energy Research [UKCMER] under the Engineering and Physical Sciences [EPSRC] SuperGen Marine Phase 3 grant Nr. EP/I027912/1. The work described in this publication was also supported by the European Communitys Sixth Framework Programme through the grant to the budget of the Integrated Infrastructure Initiative HYDRALAB III,Contract No.022441(RII3).

REFERENCES

[1] Callaghan, J., and Boud, R., 2006. Future marine energy - results of the marine energy challenge: Cost competitive-

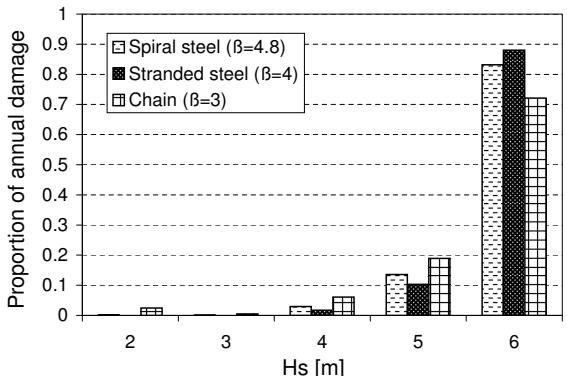

FIGURE 13. CONTRIBUTION OF DIFFERENT SEA STATES TO ACCUMULATED FATIGUE

ness and growth of wave and tidal stream energy. Tech. rep., The Carbon Trust.

[2] Department of Energy and Climate Change [DECC], 2010. Marine Energy Action Plan 2010 - Executive Summary & Recommendations. Tech. rep., HM Government.

[3] UKERC, 2007. Marine (wave and tidal current) renewable energy technology roadmap. Tech. rep., UK Energy Research Centre.

[4] Mueller, M., and Wallace, R., 2008. "Enabling science and technology for marine renewable energy". Energy Policy, **36**, pp. 4376–4382.

[5] Ricci, P., Villate, Jose, L., Scuotto, M., Zubiate, L., Davey, T., Smith, George, H., Smith, H., Huertas-Olivares, C., Neumann, F., Stallard, T., Bittencourt Ferreira, C., Flinn, J., Boehme, T., Grant, A., Johnstone, C., Retzler, C., and Sørensen, H. C., 2009. Deliverable d1.1, global analysis of pre-normative research activities for marine energy. Tech. rep., Equitable Testing and Evaluation of Marine Energy Extraction Devices in terms of Performance, Cost and Environmental Impact [EquiMar].

[6] Det Norske Veritas [DNV], 2005. Guidelines on design and operation of wave energy converters. Tech. rep., Carbon Trust.

[7] Starling, M., 2009. Guidelines for reliability, maintainability and survivability of marine energy conversion systems. Tech. rep., The European Marine Energy Centre [EMEC].

[8] Hudson, J. A., Phillips, D. C., and Wilkins, N. J. M., 1980. "Material aspects of wave energy converters". Journal of materials science, **15**, pp. 1337–1363.

[9] South West Regional Development Agency [SWRDA], 2011. Invitation to express an interest in deploying at wave hub in 2012. www.wavehub.co.uk.

[10] Bryden, I., and Linfoot, B., 2010. "Wave and current testing of an array of wave energy converters". In Proc. of the HYDRALAB III Joint User Meeting.

[11] Krivtsov, V., and Linfoot, B., 2010. "Physical model investigations of mooring loads in arrays of wave energy converters". In International Association for Hydro-Environment Engineering and Research [IAHR].

[12] Ashton, I., Johanning, L., and Linfoot, B., 2009. "Measurement of the effect of power absorption in the lee of a wave energy converter". In Proc. ASME 28th International Conference on Ocean, Offshore and Arctic Engineering.

[13] Payne, G., 2008. Guidance for the experimental tank testing of wave energy converters. Tech. rep., SuperGen Marine, The University of Edinburgh.

[14] Schijve, J., 2009. Fatigue of structures and materials. Springer.

[15] Rychlik, I., 1987. "A new definition of the rainflow cycle counting method". Int. Journal of Fatigue, **9**, pp. 119–121.

[16] Wang, K. S., Shen, Y. C., and Huang, J., 1997. "Loading adjustment for fatigue problem based on reliability considerations". International Journal of Fatigue, **19**, pp. 693 – 702.

[17] Stacey, A., and Sharp, J. V., 2007. "Safety factor requirements for the offshore industry". Engineering Failure Analysis, **14**, pp. 442 – 458.

[18] DNV-OS-E301, 2010. Offshore standard - position mooring. Standard, Det Norske Veritas [DNV], October.

[19] WAFO-group, 2000. WAFO - A Matlab Toolbox for Analysis of Random Waves and Loads - A Tutorial. Center for Math. Sci., Lund Univ., Lund, Sweden.

[20] Pitt, E., Saulter, A., and Smith, H., 2006. The wave power climate at the wave hub site. Tech. rep., Applied Wave Research report to the SWRDA.

[21] Phillips, J., Cruz, J., Rawlinson-Smith, R., Parkes, J., and Holbrow, R., 2008. "Defining the long-term wave resource at wave hub: The role of measurements and models". In Proc. of 27th Int. Conf. on Offshore Mechanics and Arctic Engineering [OMAE], no. OMAE2008-57349.

[22] Jeng, D., 2008. Ocean engineering research advances. Nova Science, New York, ch. Random wave-induced pore pressure and effective stresses in a porous seabed /, pp. 113–116.

[23] Thies, P. R., Johanning, L., and Smith, G. H., 2011. "Towards component reliability testing for marine energy converters". Ocean Engineering, **38**(2-3), pp. 360 – 370.

[24] Johanning, L., Thies, P. R., Parish, D., and Smith, G. H., 2011. "Offshore reliability approach for floating renewable energy devices". In Proc. of 30th Int. Conference on Ocean, Offshore and Arctic Engineering [OMAE], no. OMAE2011-49844.